AD-A114 812 NAVAL RESEARCH LAB WASHINGTON DC F/G 17/9
BROAD-BAND MIRROR-SCANNED SURVEILLANCE RADAR ANTENNA.(U)
APR 82 B L LEWIS, J P SHELTON, E E MAINE
UNCLASSIFIED NRL-8574 NL

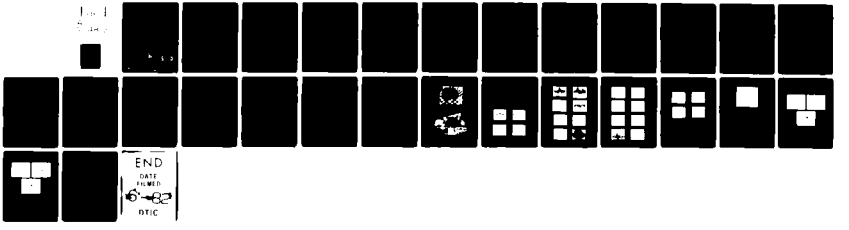

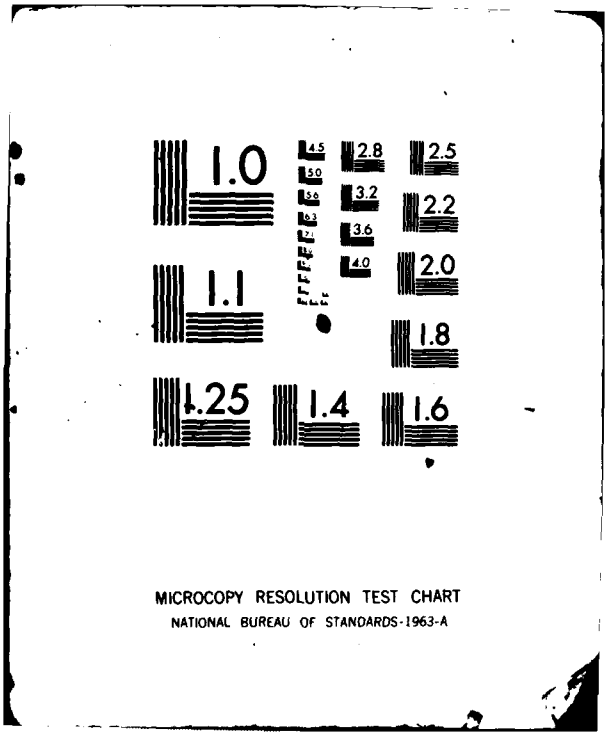
1.0
1.1
1.25
1.4
1.6
1.8
2.0
2.2
2.5
2.8
3.2
3.6
4.0
4.5
5.0
5.6
6.3
MICROCOPY RESOLUTION TEST CHART
NATIONAL BUREAU OF STANDARDS-1963-A

NRL Report 8574

Broad-Band Mirror-Scanned Surveillance Radar Antenna

B. L. LEWIS, J. P. SHELTON, E. E. MAINE,
N. V. O'NEAL, AND C. L. MOODY

Target Characteristics Branch
Radar Division

April 29, 1982

NAVAL RESEARCH LABORATORY
Washington, D.C.

SECURITY CLASSIFICATION OF THIS PAGE (When Data Entered)

REPORT DOCUMENTATION PAGE		READ INSTRUCTIONS BEFORE COMPLETING FORM
1. REPORT NUMBER NRL Report 8574	2. GOVT ACCESSION NO. AD-A114812	3. RECIPIENT'S CATALOG NUMBER
4. TITLE (and Subtitle) BROAD-BAND MIRROR-SCANNED SURVEILLANCE RADAR ANTENNA		5. TYPE OF REPORT & PERIOD COVERED Final report 6. PERFORMING ORG. REPORT NUMBER
7. AUTHOR(s) B. L. Lewis, J. P. Shelton, E. E. Maine, N. V. O'Neal, and C. L. Moody		8. CONTRACT OR GRANT NUMBER(s)
9. PERFORMING ORGANIZATION NAME AND ADDRESS Naval Research Laboratory Washington, DC 20375		10. PROGRAM ELEMENT, PROJECT, TASK AREA & WORK UNIT NUMBERS SF12-141-491 R12-14.801 53-0611-0-2
11. CONTROLLING OFFICE NAME AND ADDRESS Naval Sea Systems Command Washington, DC 20362		12. REPORT DATE April 29, 1982 13. NUMBER OF PAGES 27
14. MONITORING AGENCY NAME & ADDRESS(if different from Controlling Office)		15. SECURITY CLASS. (of this report) UNCLASSIFIED 15a. DECLASSIFICATION/DOWNGRADING SCHEDULE

16. DISTRIBUTION STATEMENT (of this Report)

Approved for public release; distribution unlimited.

17. DISTRIBUTION STATEMENT (of the abstract entered in Block 20, if different from Report)

18. SUPPLEMENTARY NOTES

19. KEY WORDS (Continue on reverse side if necessary and identify by block number)

Antennas
Surveillance radar

20. ABSTRACT (Continue on reverse side if necessary and identify by block number)

New applications and methods of broadbanding mirror scanned antennas to multioctave coverage are discussed. The applications include hemispheric coverage with pencil beams and continuous 360° azimuth scan with vertical fan beams. In these applications, a twist reflector is the only moving part so that multiple stacked beams or multiple band multifunction beams can be easily instrumented.

DD FORM 1 JAN 73 1473 EDITION OF 1 NOV 65 IS OBSOLETE
S/N 0102-014-6601

SECURITY CLASSIFICATION OF THIS PAGE (When Data Entered)

CONTENTS

BROAD-BAND MIRROR-SCANNED SURVEILLANCE RADAR ANTENNA

INTRODUCTION

Physical limitations on the number of rotary RF joints that can be used in a surveillance radar with a conventional antenna limit the number of functions that can be realized, or increase the amount of signal processing that must be accomplished on the antenna. For example, a stacked beam height finding radar must use a rotary joint with as many channels as it has beams or it must process the data on the moving antenna. The former alternative is difficult if not impossible, and the latter is unattractive because of the difficulty in maintenance and increased above-deck weight.

It is the purpose of this report to document the results of a 2-year effort directed toward avoiding the multiple-channel rotary joint problem. The goal of the effort was to determine the feasibility of applying mirror-scan techniques to broad-band multiple beam surveillance radar antennas.

ANTENNA CONCEPT

The antenna concept is an extension of the mirror-scan techniques employed in weapon control radar both in this country and abroad [1]. The principle of operation of a mirror-scanned weapon control radar antenna is illustrated in Fig. 1. A fixed vertically polarized feed illuminates a fixed parabolic reflector constructed of vertical wires. This parabola collimates the radiation and illuminates a flat half-wave plate reflector that can rotate about axes orthogonal to the optical axis of the feed and parabola. This half-wave plate rotates the plane of polarization 90° and reflects the resultant radiation at an angle of reflection equal to the angle of incidence. With the E field normal to the wires in the parabola, the reflected radiation goes right through the parabola as if it were not there. In this application, the beam is steered (scanned) by controlling the orientation of the flat half-wave plate reflector.

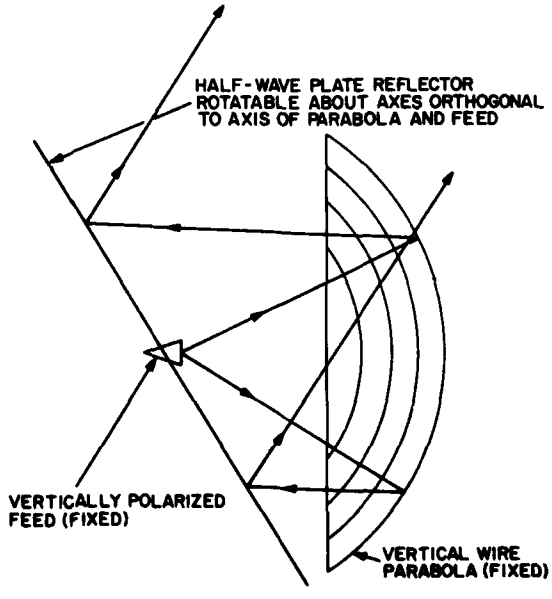

Fig. 1 — Mirror-scanned radar antenna

Manuscript submitted December 4, 1981.

It should be noted that, as long as the half-wave plate reflector intercepts the complete beam from the parabola, there is no scan loss and no beam shape deterioration with varying scan angles. It should also be noted that the scan angle of the beam is twice the angle the feed-parabola optical axis makes with the half-wave plate reflector. Thus, a beam deflection from 0 to 90° requires a plate rotation of only 45°. As a consequence, a plate $\sqrt{2}$ times larger than the parabola aperture in the plane of scan can be used to scan a beam through plus and minus 90° (a total of 180°) without gain loss.

Figure 2 illustrates one method of obtaining a 360° scan using the mirror-scan concept. Two parabolas and two feeds are used with a double sided rotating half-wave plate reflector. Both feeds are excited while the rotating reflector is within plus and minus 45° of normal to the feed-parabola optical axis and opposite hemispheres are scanned simultaneously. However, neither feed can be excited for the rest of the reflector scan cycle because the foreshortening of the rotating reflector produces excessive spillover loss with reasonable reflector sizes.

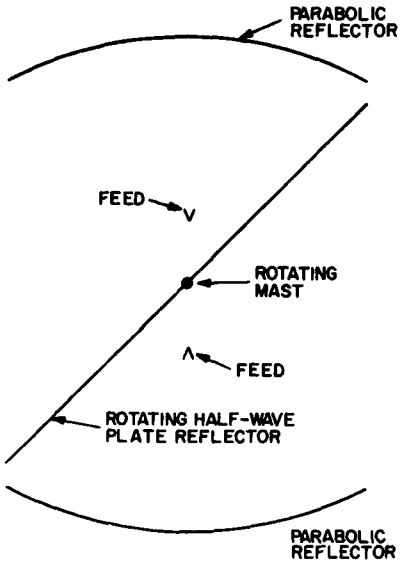

Fig. 2 — Extension of mirror scan concept to 360° azimuth coverage

Figure 3 illustrates a method of instrumentation that will permit full-time operation. In this case, four parabolas and four feeds can operate in pairs to scan 360° four times per revolution of the rotating reflector. Figure 4 shows that feeds 1 and 3 can scan 180° through 90° to 0° and 0° through 270° to 180° simultaneously for 1/4 of a reflector scan period. Then, feeds 2 and 4 scan 90° to 270° and 270° to 90° the next 1/4 of the reflector scan period. Thus, four complete 360° azimuth scans can be made in one mirror rotation.

If back-to-back scans are not desired, each feed and parabola can be used to scan 90° and the rotating reflector length can be reduced from $\sqrt{2}A$ to $1.082A$, where A is the parabola length in the scan plane. However, this will result in dead times between 90° scans equal to the time required for the rotating reflector to move 45°. Actually, a certain amount of dead time is desirable to permit feed switching to be accomplished.

Figure 5 is a side view of the four-parabola system illustrating how offset feeds can be used to avoid physical interference of the feeds and the rotating reflector. It should be noted that multiple feeds can be used in this configuration to obtain stacked beams for height finding without using continuously rotating joints.

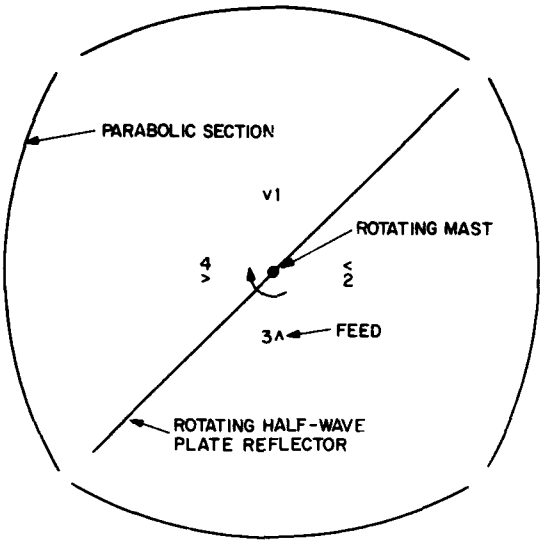

Fig. 3 — Top view of antenna scanning 360° in azimuth with no rotating RF joints

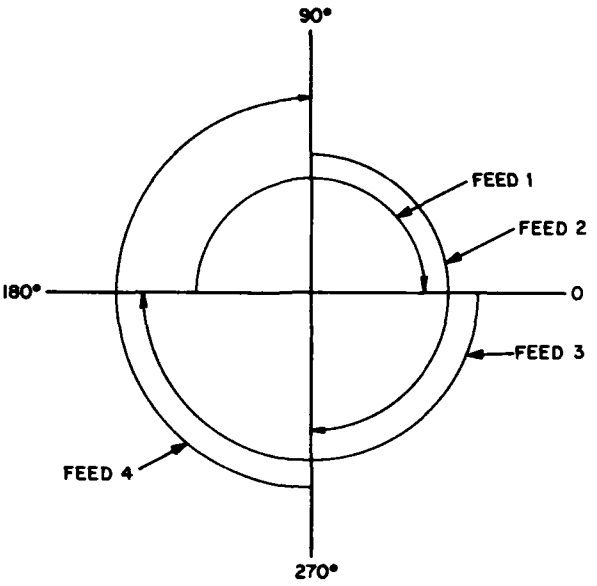

Fig. 4 — Scan angles available per feed from one side of half-wave plate reflector with no scan loss if reflector is 41.4% longer than parabolic section

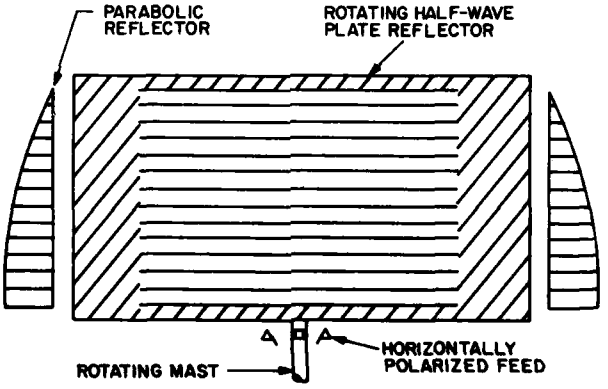

Fig. 5 — Side view of antenna illustrating feed placement

It is obvious at this point that eight feeds and eight parabolas with a smaller rotating reflector could be used to obtain full-time coverage and 360° continuous or back-to-back scans with each feed covering 45°. However, such a system would get uncomfortably large at long wavelengths for shipboard applications, although it might be very practical for a rapid scanning high-frequency last-ditch radar for use against pop-up targets.

ACHIEVABLE BANDWIDTH

The bandwidth achievable with the proposed system can be quite large (10 to 1 or greater). The parabolas have no restrictions except wire spacing that sets the high-frequency limit and the half-wave plate reflector can be made to cover many octaves by employing a log periodic distribution of reflecting dipoles. These elements would be distributed in depth to produce a 180° path length difference between the front surface reflection and the orthogonal back surface reflection over any desired band.

LIGHT-WEIGHT CONSTRUCTION

The proposed antenna lends itself to light-weight construction techniques. The parabolas can be linear parallel conductors printed or glued onto the inside surface of a fiberglass coated foam structure and the half-wave plate can be linear conductors in a fiberglass coated foam sheet. The parabolic structures can be extended to meet each other to form the walls of a radome and a fiberglass on foam top can be added if desired.

An idea of the weight involved in a high-gain L-band antenna can be obtained as follows:

Assume that each parabola is 12 × 20 ft. To rotate a reflector 1/cos (45°) longer than 20 ft between the parabolas, the parabolas will have to be separated from their opposite number by about 28 ft. This structure can be approximated by a square 28 ft across and 12 ft high. If the parabolas are taken to be 2-in. thick and coated on both sides with 0.012-inch-thick fiberglass, the foam volume will be:

$$V_F = 4 \times 1/6 \times 28 \times 12 = 224 \text{ cu ft},$$

and the volume of fiberglass will be

$$V_g = 4 \times 28 \times 12 \times 2 \times 0.001 = 2.69 \text{ cu ft}.$$

With foam densities of 3 pounds per cu ft and fiberglass densities of 125 lb per cu ft, the weight will be

$$W = 224 \times 3 + 2.69 \times 125 = 1008 \text{ lb}.$$

The foam and fiberglass in the half-wave plate reflector can be held to volumes on the order of

$$V_{SFR} = 1/6 \times 12 \times 28 = 56 \text{ cu ft}$$

for structural foam, and

$$V_{FR} = 1/3 \times 12 \times 28 = 112 \text{ cu ft}$$

of filler foam with

$$V_{gR} \approx (2 \times 28 + 2 \times 12 + 2 \times 12 \times 28)0.001 = 0.752 \text{ cu ft}$$

of fiberglass. This would result in a half-wave plate reflector weight of

$$W_R = 56 \times 3 + 112 \times 1 + 0.752 \times 125 = 374 \text{ pounds}$$

where the filler foam density was taken to be one lb per cu ft.

Allowing 8 each 1 ft × 28 ft × 1/4 ft braces (4 on the top and 4 on the bottom) will add

$$V_{BF} = 8 \times 1 \times 28 \times 1/4 = 56 \text{ cu ft},$$

$$V_{Bg} = (2 \times 8 \times 28 \times 1 + 2 \times 8 \times 1/4 \times 28)\ 0.001 = 0.56 \text{ cu ft},$$

and weight

$$W_B = 56 \times 3 + 0.56 \times 125 = 238 \text{ lb}.$$

The total structural weight will be

$$W_S = 1620 \text{ lb}.$$

This weight is comparable to that of present day antennas of equivalent gain, the rotating mass is significantly less and the structure provides a wind screen for the rotating reflector.

The addition of a top cap to complete the wind screen and to act as a weather shield would add approximately 700 lb if it were composed of 2-inch-thick foam coated on both sides with 0.012-inch-thick fiberglass. This would provide a complete radome and increase the weight to about 2300 lb.

FREQUENCY SCALING

The size and weight of the structure required to produce equal gain antennas can be scaled inversely with frequency. For example, an *S*-band version would be 1/3 the size and about 1/10 the weight of the *L*-band model previously discussed.

HEIGHT FINDER MODIFICATIONS

The use of the proposed antenna as a height finder with vertically stacked beams would require an increase in the reflector height of $B \tan \phi$, where ϕ is the elevation angle of the top beam and B is the distance between the parabola vertex and the most distant point on the half-wave plate reflector in its scan cycle.

Relatively large focal length to diameter ratios (on the order of 0.5) are possible in this antenna without increasing the parabola spacings over those required to permit half-wave plate reflector rotation. This implies that up to seven beams could be stacked in azimuth and more in elevation without experiencing excessive gain loss [2].

POLARIZATION EFFECTS

The curvature and the finite focal length F of the parabolas will introduce a small amount of spill-over loss on transmission that will appear as blockage on reception due to polarization effects if the parabola uses horizontal wires. This can be understood through reference to Fig. 6 which illustrates how a parabolic reflector composed of horizontal wires will appear to the feed at the focal point of the parabola. The wires projecting into the dimension parallel to the axis of the parabola (X) will appear to the feed to have a vertical component in Y if both Y and Z are not zero at the point in question. An idea of the magnitude of this effect can be obtained as follows:

The equation defining the shape of a parabolic reflector with a focal length F whose axis is parallel to the X axis is

$$X = (Y^2 + Z^2)/4F = P^2/4F. \tag{1}$$

Since the conductors making up the parabola were considered to be horizontal, the projection of the wires in the X dimension will be a function only of Z if Y is taken to be vertical. Thus,

$$dX/dZ = Z/2F \tag{2}$$

and, at any point Z

$$dX = ZdZ/2F. \tag{3}$$

Seen from the feed, dX will project on the Y, Z plane as

$$dP = dX\ [P/(F - X)]. \tag{4}$$

This projection will have a Y component

$$dY = dP\ [Y/(Y^2 + Z^2)^{1/2}]. \tag{5}$$

Hence, at a point X, Y, Z on the parabola, the wire will appear to have a finite slope in Y with respect to Z of

$$dY/dZ = 2YZ/[4F^2 - (Y^2 + Z^2)]. \tag{6}$$

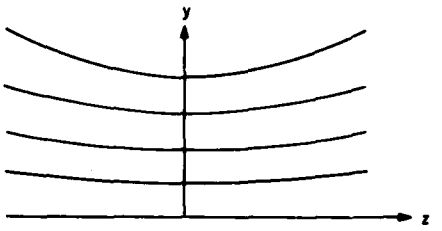

Fig. 6 — Horizontal wires in parabola seen from feed

If rectangular reflectors were used with

$$Z_{max} = 0.8F \text{ and } Y_{max} = F, \tag{7}$$

the maximum value of dY/dZ will be

$$dY/dZ = 0.678. \tag{8}$$

This apparent projection of the wire into the Y direction will limit the reflection coefficient of the reflector at this point to horizontally polarized radiation from the feed to $(1 - 0.678^2)^{1/2} = 0.72$ at the point in question and will permit spillover of 0.46 of the incident power. This is not too significant since the illumination will be heavily tapered at this point and the power lost would have gone into cross-polarized lobes from a conventional antenna in any case.

This spillover could be avoided if the wires making up the parabola were given a Y component opposite that portrayed in Fig. 6. However, such a step would partially reintroduce the blockage to the signal reflected by the half-wave plate reflector for horizontal radiation patterns. Proper curvature of the wires in Y would reduce the reflector blockage to plane waves entering from elevation angles greater than zero, however, and should be considered in more detailed design if height finding is anticipated.

VARIATION OF HALF-WAVE PLATE EFFICIENCY WITH SCAN ANGLE

One final polarization problem involves the half-wave plate reflector. The effective spacing between orthogonal reflecting planes must be kept nearly equal to $\lambda/4$. This condition is violated at scan angles such that the radiation impinges on the half-wave plate at angles of incidence on the order of 45°. However, refraction can be used to limit the angle of incidence on the back reflecting surface by loading the region between reflecting planes with an artificial dielectric. A dielectric constant of 2 will limit depolarization loss to less than 0.6 dB at scan angles such that the angle of incidence on the half-wave plate is 45°.

BEAM STABILIZATION

The beam or beams from this antenna can be stabilized in level by rotating the half-wave plate reflector about a horizontal axis through its center as illustrated in Fig. 7.

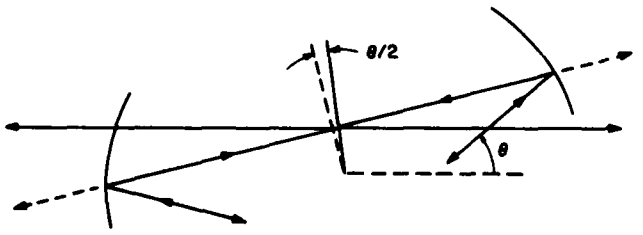

Fig. 7 — Level stabilization of θ via mirror rotation through $\theta/2$

Cross-level coupling between azimuth and elevation can be corrected by data stabilization because of the high data rate available from this antenna. The antenna can make many scans in the roll or pitch period of the ship. This data can be compared to an inertial reference system to detect azimuth changes with cross-level changes. These azimuth changes will be directly proportional to target elevation angle and will permit target elevation to be measured with a 2-D radar. With knowledge of elevation and cross level, the true azimuth of a target can be calculated [3].

ADVANTAGES AND DISADVANTAGES

Advantages

The advantages that the proposed antenna would have over conventional antennas are:

1. No continuously rotating RF joints are required.

2. The structure provides its own radome and the rotating reflector is protected from all wind loads.

3. All aperture blockage by feeds can be eliminated to obtain low sidelobes.

4. The rotating structure is light in weight and has minimum moment of inertia for its task.

5. High scan rates are achievable due to the scan angle multiplication at the rotating reflector. Four 360° scans are obtained per reflector rotation.

6. Multiple beams stacked in azimuth and elevation can be used without adding inertia to the rotating structure, aperture blockage or continuously rotating RF joints. It is much less complex than an array that would perform the same function. All signal processing can be performed below decks.

Disadvantages

The disadvantages of this type of antenna over other types that would scan the same angle are:

1. The turning circle of the reflector is about 40% larger than would be required for normal antennas having the same gain.

2. Two receivers and data processing are required to obtain continuous data and to adapt this data to conventional displays.

UNIPOLAR PARABOLA DESIGN

The unipolar parabolas are constructed of foam-filled fiberglass with parallel vertical conductors on or in the surface. Efficient operation can be obtained at any frequency at which the conductor spacing is less than or equal to 0.1 wavelength of the radiation involved and the conductor width is on the order of 0.05 wavelength at the highest frequency of interest. In addition, the conductor depth must be several times the skin depth at the lowest frequency of interest.

Tests were made with 2 mil-thick copper conductors on 1/32 in. thick fiberglass with 1/32 in. conductor widths and 1/8 in. center-to-center spacings. Reflection coefficients of 0.95 or greater were obtained when the incident radiation was polarized parallel to the conductors and the frequency was below 12.4 GHz. When the radiation was polarized normal to the conductors, the reflection coefficient was less than 0.05.

HALF-WAVE PLATE MIRROR BANDWIDTH CONSIDERATIONS

The description of the mirror scan antenna given in previous sections calls for a rotating half-wave plate reflector. The effect of this reflector is to rotate the polarization of the wave incident on it by 90° from vertical to horizontal. The purpose of this section is to discuss possible techniques for achieving this required half-wave plate operation.

In general, the polarization rotation is obtained by making the reflection coefficient of the mirror surface polarization dependent, as shown in Fig. 8(a). Two linear polarization components are used, one aligned at +45° to the vertical and the other at −45°. The reflection coefficient for one of the components can be represented by $\rho_1 = e^{j\phi}$, and the coefficient for the other one will be $\rho_2 = -\rho_1 = -e^{j\phi}$ or $e^{-j(\phi+\pi)}$.

Figure 8(b) shows the decomposition of an incident vertically polarized wave into ±45° components. It is seen that upon reflection the components have reversed their relative signs, and the reflected wave is horizontally polarized.

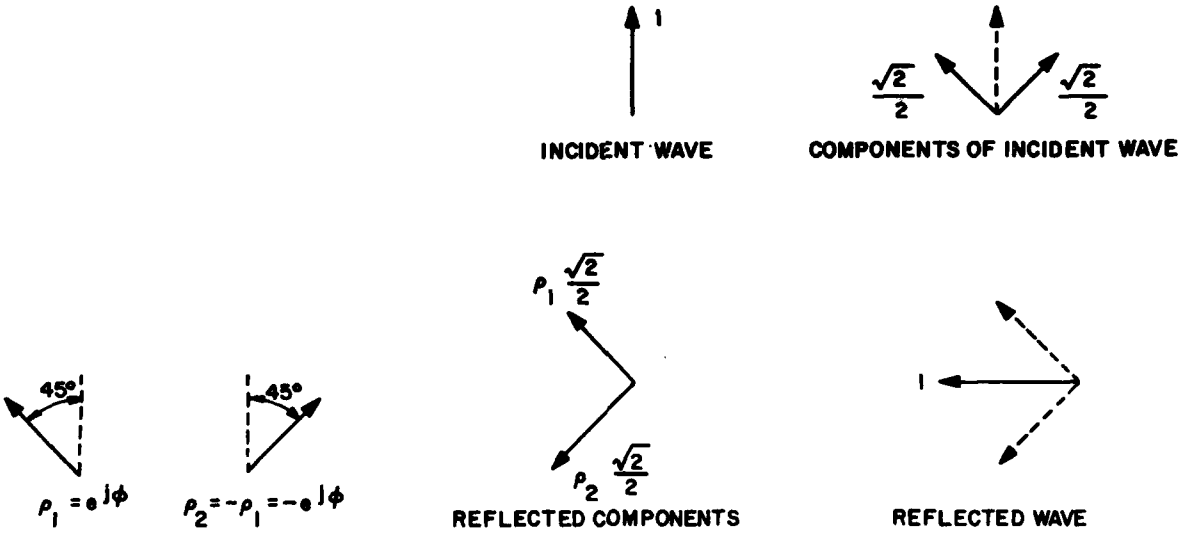

(a) Polarization-dependent reflector

(b) Reflected components from reflector

Fig. 8 — Operation of polarization twist reflector

The half-wave plate reflector has also been referred to as a twist reflector [4].

Three techniques for designing a half-wave plate reflector are discussed in this report. These techniques are distinguished primarily by their operating bandwidths. One technique is relatively narrow-band, with bandwidth well under one octave. The second has bandwidth of roughly one octave, and the third has wide bandwidth capability of multiple octaves.

The most commonly used technique for realizing a half-wave plate or twist reflector is to place a closely spaced wire grid about $\lambda/4$ in front of a reflecting surface. A wave polarized parallel with the wire grid will reflect from the grid, and a wave polarized perpendicular with the grid will pass through the grid and reflect from the surface, with a net phase difference between components of π. Since this phase difference is based on path length, it is frequency sensitive.

The theoretical conversion efficiency of the wire grid configuration is

$$E_\rho = \cos^2\left[\frac{\Delta f}{f_0}\,\frac{\pi}{2}\right],$$

where E_ρ is the fraction of incident power that is twisted to the desired output polarization, f_0 is the design frequency, and Δf is the deviation from design frequency.

A technique with moderately wide bandwidth involves the use of a meander-line quarter-wave plate in front of a reflecting surface. On its forward passage through the quarter-wave plate, the orthogonally polarized components undergo a $\pi/2$ phase difference, and the wave is circularly polarized. Upon reflection from the surface and after its second passage through the quarter-wave plate, the components undergo an additional $\pi/2$ relative phase shift, providing the desired half-wave plate characteristics [5]. (This application of a reflector-backed-meander-line quarter-wave plate was suggested by D. Munger of the Naval Ocean Systems Center.)

In the course of this exploratory research program, a new design for a wideband half-wave plate reflector was conceived [6]. This design is based on log-periodic resonant structures and therefore can be built with arbitrarily wide bandwidth. This concept is described in the following section.

In initial experimental work on the mirror scan antenna, a narrow-band wire-grid half-wave plate mirror was used. All subsequent work was devoted to the design, fabrication, and test of the wideband log-periodic mirror concept.

WIDEBAND LOG-PERIODIC TWIST REFLECTOR CONCEPT

This concept for a log-periodic twist reflector is based on the use of planar arrays of resonant conducting strips or wires. Each array consists of a regular lattice of identical resonant conducting strips or wires, as shown in Fig. 9. Assuming that the planar array is aligned with the X-Y plane, a log-periodic configuration is obtained by layering the planar arrays in the Z dimension. The spacing of the layers is log periodic in the Z dimension, and all dimensions of the planar arrays are correspondingly scaled in the same log-periodic fashion. Figure 10 is a cross section of a log-periodic mirror structure in the X-Z plane. The operation of the resulting three-dimensional log-period lattice is analogous to that of log-periodic circuits described by DuHamel [7]. A plane electromagnetic wave enters the lattice on the side with smallest parasitic strips and travels in until it encounters resonant strips, where it is reflected. The magnitude of the reflection coefficient of the structures is theoretically unity, and the phase of the reflection coefficient varies essentially linearly with the logarithm of frequency

$$\phi = K_1 \log\left[K_2\,\frac{f}{f_0}\right], \tag{14}$$

where f_0 is a reference frequency, $K_1 = 2\pi/\log\tau$, τ is the scale factor from one layer to the next, and K_2 is a constant which depends on the scale of the overall structure.

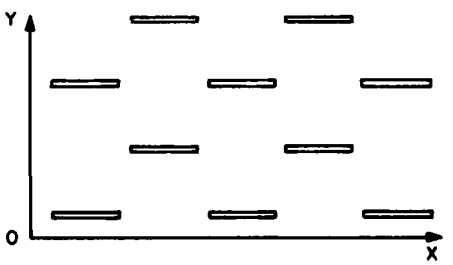

Fig. 9 — Planar array of resonant conducting wires or strips

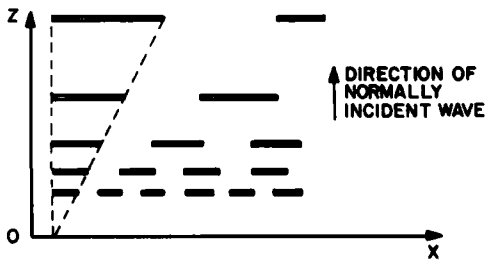

Fig. 10 — X-Z cross section of log-periodic 3D lattice

To achieve polarization transformation, it is necessary to use orthogonally polarized log-periodic lattices. These lattices use the same coordinate systems as shown in Figs. 9 and 10 and the same scale factor τ.

That is, the reflection coefficients of the two lattices can be expressed, without loss of generality,

$$\phi_{+45^\circ} = K_1 \log \frac{f}{f_0}$$

and

$$\phi_{-45^\circ} = K_1 \log K_2 \frac{f}{f_0}.$$

The phase difference between reflection coefficients will be

$$\Delta\phi = \phi_{-45^\circ} - \phi_{+45^\circ} = K_1 \log K_2$$
$$= \frac{2\pi \log K_2}{\log \tau}. \tag{15}$$

Therefore, the phase difference between reflection coefficients of vertical and horizontal polarization is frequency-independent, and we have the basis for wideband operation. For a half-wave plate, or twist-reflector, we require $\Delta\phi = \pi$, and Eq. (15) gives

$$K_2 = \tau^{1/2},$$

that is, the scale factor between the orthogonally polarized lattices is $\tau^{1/2}$ so that the resonant layers of one lattice are located at values of the Z coordinate which are geometric means of the locations of the layers of the other lattice.

Although the wideband log periodic half-wave plate is analogous to the log-periodic circuits proposed by DuHamel, there are differences and additional problem areas as well as similarities.

A basic characteristic of DuHamel's log-periodic stub-loaded transmission line is that any energy passing through the initial resonance region is inevitably refleted back to the input with a delecterious effect on the reflection phase coefficient. This is because the network is lossless and wholly reactive. This effect exhibits itself by very rapid changes of reflection phase through increments of 2π radians. Since all of DuHamel's analysis was empirical, using computer simulation, with finite networks, one might conjecture that an infinite network might exhibit a completely discontinuous reflection phase function.

Fortunately, however, the phase discontinuity problem is largely eliminated by introducing transmission line loss at a level which is encountered in practical networks. Similar losses can be expected in the log periodic polarization twisting mirror. Furthermore, the mirror is a 3-D structure with attendant additional characteristics over and beyond those of the network. The regular periodic lattice of any given layer makes it possible for waves to be scattered other than specularly, especially after the incident wave has passed through the initial resonance region; that is, once a plane wave falls on a layer of parasitic dipoles, those dipoles behave on reradiation exactly as a phased array. If the dipole spacing is sufficiently large relative to a wavelength, the reradiated energy diffracts into grating lobes as well as a specular lobe. This phenomenon is to be avoided at the initial resonance region, where only specular reflection with no grating lobes is mandatory for proper performance. As the wave progresses deeper into the structure and the scale of layers becomes larger, grating lobes become unavoidable. Furthermore, grating lobe reradiation can be viewed as a form of attenuation and is acceptable and even desirable for energy passing through the resonance region.

Another aspect in which the mirror differs from the network is with regard to variation in incidence angle. A thorough analysis of the behavior of the mirror must include the case of oblique incidence.

Finally, both the network and the mirror exhibit a characteristic impedance, which differs from the main transmission line for the network and differs from the impedance of free space for the mirror. For the network this is easily reconciled by designing the network to whatever input impedance is required. For the mirror it is not possible to obtain an arbitrary input impedance, and it will be necessary to impedance transform from space to the interior of the mirror.

SCAN ANGLE COMPENSATION

The effect of scan angle on a normal half-wave plate can be determined as follows.

Figure 11 illustrates a simple two-plane half-wave plate reflector with an electromagnetic wave incident on it at an angle of incidence θ. The first plane hit by radiation is composed of parallel conductors making an angle of 45° with the incident E field. These conductors are about 0.05 wavelength wide at the highest frequency of interest and are separated center-to-center by 0.125 in.

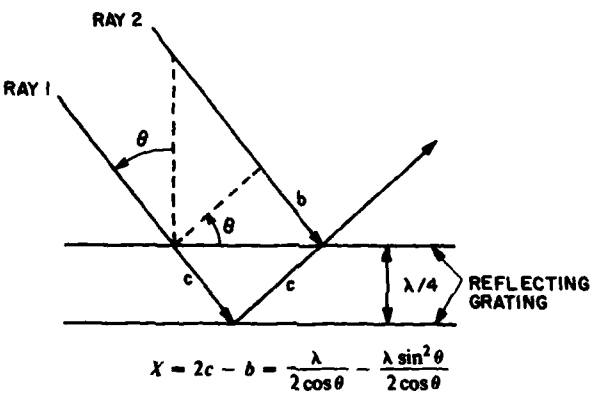

Fig. 11 — Effect of scan angle on normal half-wave plate

The second plane hit has the same type of conductors but orthogonal to those in the first plane. The two planes are separated by a distance of 1/4 wavelength ($\lambda/4$) of the desired band center frequency. The component of ray 1 polarized normal to the conductors in the first plane passes through the first plane as shown. It reflects from the second plane since its conductors are parallel to the incident E field (orthogonal to those in the first plane). The component of ray 1 that reflects from the second plane passes through the first plane and combines vectorially with the component of ray 2 that reflects from the front plane with a path length difference

$$X = 2c - b = \frac{\lambda}{2\cos\theta} - \frac{\lambda \sin^2\theta}{2\cos\theta} \text{ or}$$

$$X = \frac{\lambda}{2\cos}(1 - \sin^2\theta) = \frac{\lambda\cos\theta}{2}.$$

When $\theta = 0°$, $X = \lambda/2$ and the system is a perfect half-wave plate reflector. The two orthogonally polarized components of the incident radiation add with 180° phase differences to form a wave polarized normal to the incident wave. However, when $\theta = 45°$, $X = \frac{\lambda}{2\sqrt{2}}$ and the resultant phase difference on addition is only 138° rather than 180°. This 42° phase error in θ results in a desired polarization rotation efficiency of

$$G = \cos^2(\theta/2) = 0.87 \approx -0.6 \text{ dB}.$$

When θ is 90°, the half-wave plate reflector becomes a quarter-wave plate reflector and converts linear polarization to circular polarization.

The scan loss at $\theta = 45°$ due to incomplete polarization rotation can be reduced by loading the region between the two reflecting planes with a material having a dielectric constant of 2 which can also serve to separate the reflecting planes [8]. Figure 12 illustrates this condition. With this loading the radiation passing plane 1 refracts at the air dielectric interface to obtain an angle of incidence on the second plane define by

$$\sin \theta_2 = \frac{\sin \theta_1}{\sqrt{2}}.$$

For $\theta_1 = 45°$, $\theta_2 = 30°$ and $G = \cos^2(15°) = 0.92$.

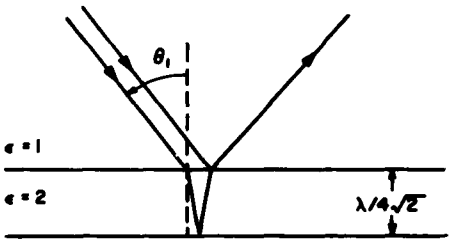

Fig. 12 — Effect of dielectric loading in normal half-wave plate

The scan loss at $\theta = 45°$ can also be reduced by increasing the reflecting plane separations to make the loss at $\theta = 45°$ equal the loss at $\theta = 0$. Under these conditions, with dielectric loading, the lowest gain will be $G \approx 0.98$. This would involve increasing the reflecting plane spacing by about 7.5° or $\lambda/48$.

An extensive experimental design program was conducted to demonstrate the feasibility of the log-periodic mirror-scan concept. This program consisted of the following phases:

a. Experimental design of a polarization twisting log-periodic mirror.

b. Fabrication and test of a scanning antenna consisting of two offset paraboloidal reflectors and a log-periodic mirror, with feed horns installed and fed simultaneously by two radars, operating at *C*- and *X*-bands.

EXPERIMENTAL DESIGN OF A LOG-PERIODIC MIRROR

At the time the wideband log-periodic polarization twist mirror was designed, computer analytic techniques for a theoretical design procedure were not available to the project. Therefore, an experimental design program was conducted.

The first step in this experimental program was to fabricate a set of reflective dipole lattices. Ideally, the dipole density for a given resonant reflecting sheet would be varied until a specified performance could be achieved. Actually, the cost of fabricating the experimental configurations was so high that only a limited range of experimental parameters could be tried.

At the outset, a very dense dipole lattice for a resonant frequency of 8 GHz was drafted and photo-etched onto a copper-clad 0.015 in.-thick epoxy glass dielectric sheet. The measurement procedure for determining the reflectivity of this sheet is sketched in Fig. 13. Transmit and receive horns

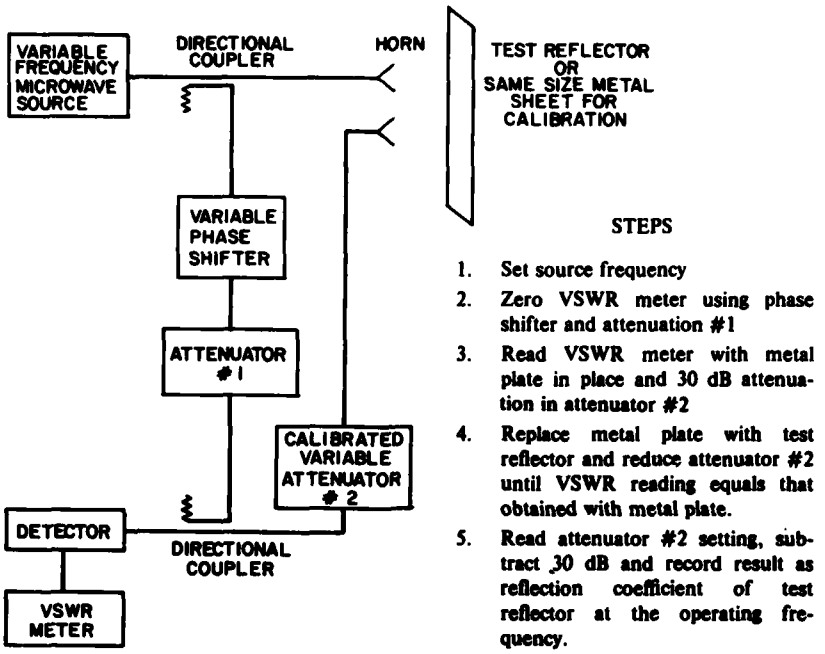

Fig. 13 — Measurement procedure for determining sheet reflectivity vs frequency

are mounted side by side, aimed at the center of a dipole lattice measuring about two ft square. When the dipole sheet is replaced by a metal sheet, the signal level is restored to its previous value by inserting calibrated attenuation. In this manner the reflectivity of the dipole sheet is measured over a wide frequency range, and its resonant frequency and bandwidth are determined.

The resonance of this structure was extremely broad, and it was decided to measure sheets with lower dipole density. This reduced density was achieved by removing vertical rows of dipoles from the initial array; thus, densities of 1/2, 1/3, and 1/4 the original densities were tried. The 1/3-density dipole configuration, shown in Fig. 14 was selected as the preferred one for use in fabricating the wideband polarization twist mirror. This configuration yields a dipole density of about 2 per square wavelength at the resonant frequency.

The next step in the design procedure was to select the scale factor between adjacent resonant sheets, τ, and the spacing between a given set of resonant sheets. The design trade-off is between minimum thickness for the overall mirror assembly and best possible performance. The parameters selected for the wideband mirror configuration are listed in Table 1, and correspond to a τ of 1.414.

The parameters in Table 1 will produce a wideband log-periodic mirror which will operate on a linearly polarized wave. In order to achieve the desired polarization twist capability, a second, orthogonally polarized log-periodic mirror must be interleaved with the mirror of Table 1. For a mirror which twists horizontal to vertical polarization or vice versa, the dipoles in the othogonally polarized mirrors are aligned at 45° to the right or left of vertical. The resultant parameters for the polarization-twist configuration are listed in Table 2.

Photographic scaling of the reference 8 GHz section (Fig. 14) was used during the photo etching process to scale the lattice and dipole parameters for other required resonant sheets. A summary of the final dipole array parameters is given in Table 3.

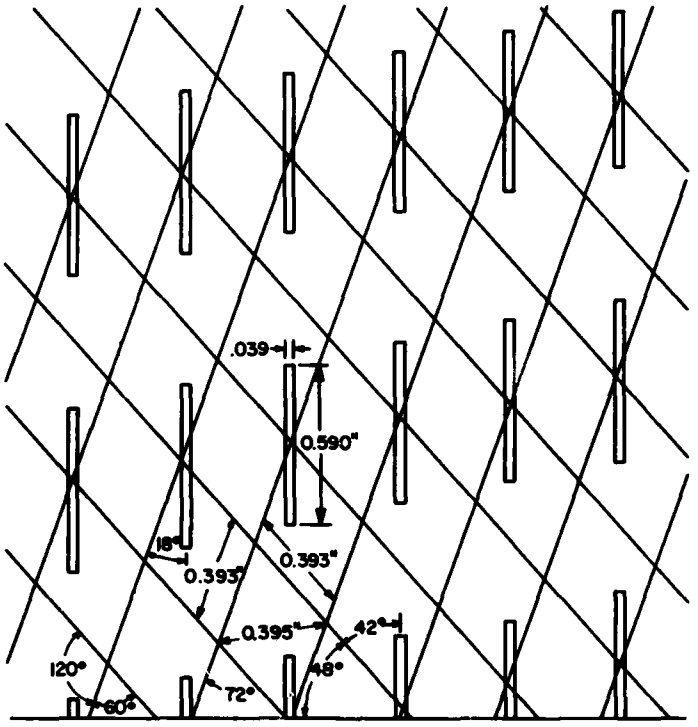

Fig. 14 — Dipole and lattice parameters for the 1/3-density 8-GHz reference sheet

Table 1 — Parameters of a Log-Periodic Mirror Operating on a Linearly Polarized Wave

Sheet Number	Resonant Frequency (GHz)	Spacing From Front Plane (in.)	Spacing Between Sheets (in.)
1	11.3136	0	
			0.313
2	8.0	0.515	
			0.442
3	5.657	1.041	
			0.626
4	4.0	1.381	

Table 2 — Parameters of Log-Periodic Polarization Twist Mirror

Sheet Number	Resonant Frequency (GHz)	Spacing from Front Plane (in.)	Spacing Between Sheets (in.)	Polarization
1	11.3136			+45°
			0.142	
2	9.514	0.1430		−45°
			0.169	
3	8.0	0.3120		+45°
			0.201	
4	6.7272	0.5130		−45°
			0.239	
5	5.657	1.7520		+45°
			0.284	
6	4.757	1.0360		−45°
			0.338	
7	4.0	1.3740		+45°
			0.402	
8	3.3636	1.7760		−45°

Table 3 — Dimensions of the Dipole and Lattice Structure for the 8 Section Log Periodic Mirror

Sheet Number	Resonant Frequency (GHz)	Dipole Length (in.)	Dipole Width (in.)	Lattice Dimension S, (in.)	Scaling Factor
1	11.3136	0.417	0.028	0.278	0.707
2	9.514	0.496	0.033	0.331	0.841
3	8.0	0.590	0.039	0.393	1.000
4	6.7272	0.702	0.047	0.468	1.189
5	5.657	0.834	0.056	0.556	1.414
6	4.757	0.992	0.066	0.662	1.682
7	4.0	1.180	0.079	0.787	2.000
8	3.3636	1.403	0.094	0.936	2.378

Test sheets measuring about 60 cm square were fabricated. The variation in measured reflectivity as a function of frequency for the individual sheets is shown in Fig. 15. The configuration of Table 2 was then assembled and tested.

The prototype NRL two-reflector mirror-scan antenna was sent to NOSC in 1977, where it was carefully tested. The results of that test program are described in NOSC Technical Note 641, by A. D. Munger [9].

EXPERIMENTAL PROTOTYPE MODEL

A working system was constructed and assembled to demonstrate the feasibility of the mirror scan concept. Implementation plans for the prototype model were held to the minimum necessary to support initial test and evaluation. The parabola and mirror designs were based on the parameters developed during the experimental design study. Only two of the four parabolas necessary for the

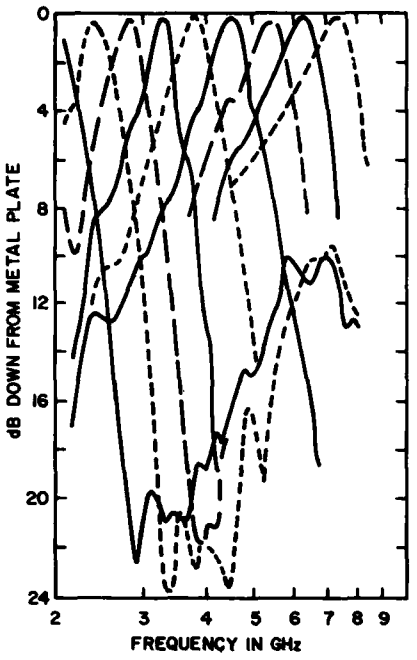

Fig. 15 — Individual sheet reflectivities for the 1/3-density dipole configuration

operational system would be implemented. This would permit the demonstration of system performance up to beam scan angles of ±90° off each parabola and the back-to-back scanning capability over the 90° sector between the two adjacently installed parabola-feed combinations. Although the parabola and mirror design would support wide-band operation, only two radars would be assembled and installed to demonstrate simultaneous system operation at *C* and *X*-bands.

An available 5-foot solid dish parabola was selected as the model for use in fabricating the two, 2- × 4-ft, unipolar parabolic sections. A fiberglass shell of the dish was fabricated. A grid of vertical conductors composed of 1/16 in.-wide printed circuit strips was installed with a nominal spacing of 1/8 in. on the rear of the shell. Foam and a second fiberglass shell were added for protection and rigidity. The two (2 ft × 4 ft) parabolic sections were then cut as shown in Fig. 16. Two matching *C*- and *X*-band horns were designed, fabricated and tested in a side-by-side configuration with the parabolic sections. Nonmetallic structures were built to attach each of the parabola-feed combinations to the selected pedestal.

Fabrication techniques for the 3 ft × 6 ft mirror were basically the same as those used during the experimental design phase. The 8-GHz mask was again used as the reference to scale photographically each of the eight resonant sections of the mirror. Since the available photo etching facility could not process sheets of this size, each section was assembled from three 2 ft × 3 ft printed sheets. The photographic process provided a convenient medium to assure proper alignment and orientation of the printed circuit dipoles at the vertical intersections between the adjoining sheets. No special efforts were made to assure continuity of any dipoles spanning the sheet intersections. Dielectric spacers were used between adjacent resonant sections during assembly. The interior voids were foam-filled and the entire assembly was wrapped with fiberglass and sealed for protection and rigidity. A metal frame was fabricated to support and permit installation of the mirror structure on the antenna pedestal. The completed system is shown in Fig. 17.

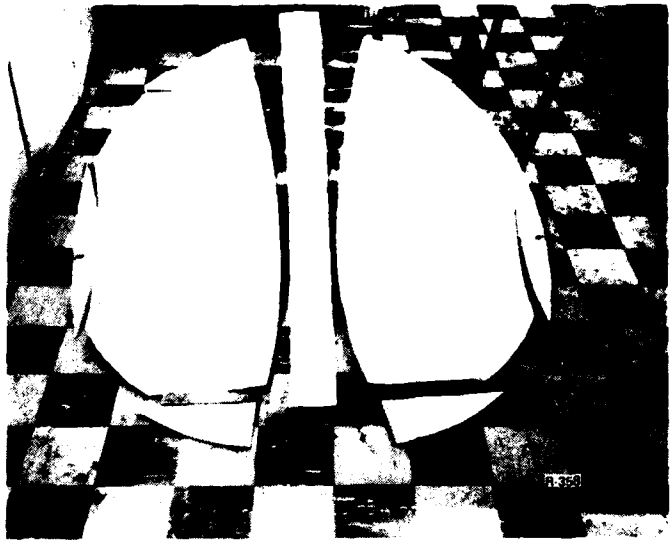

Fig. 16 — Unipolar parabolas fabricated for the prototype system

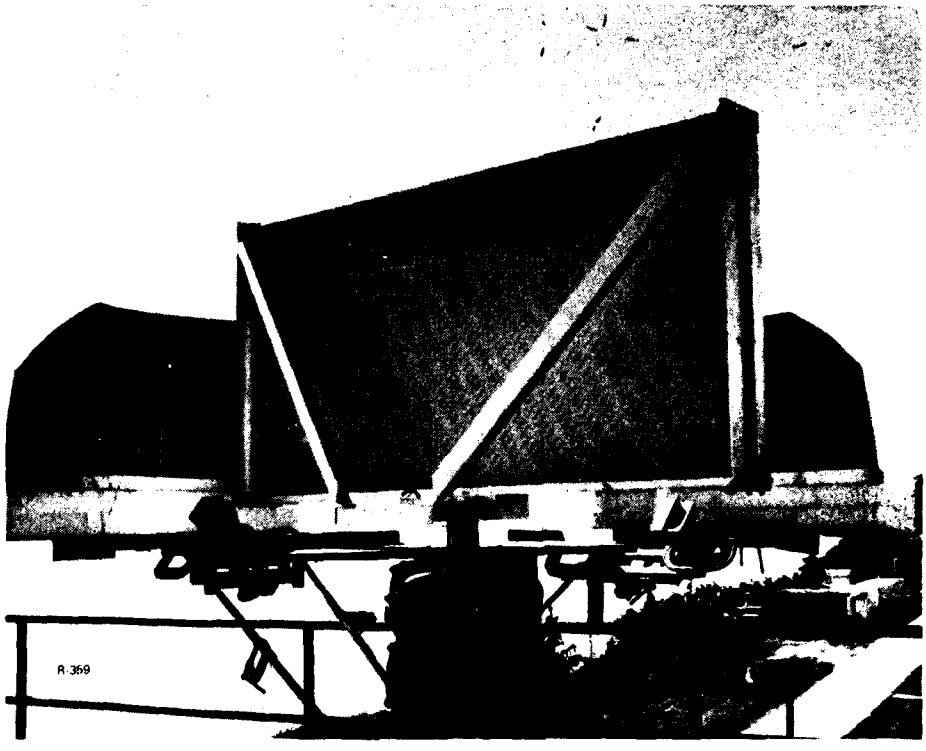

Fig. 17 — Prototype mirror scan antenna

After alignment, azimuth patterns over the frequency bands of interest were taken at fixed mirror scanned angles of 0°, 30°, 60° and 90°. Representative patterns are shown in Figs. 18 through 23. In these figures, the abscissa covers a range of approximately 180° in azimuth and the ordinate scale is 10 dB per division. In general, the sidelobes were 20 dB or more below mainlobe response. The apparent large sidelobes seen at 90° in some of the patterns were due to reflections from a nearby structure. The transmitting sources used to run these patterns showed considerable variations in output power with frequency. This is most evident at the higher frequencies where the power is marginal and the sidelobes are down in the measurement noise. A second attempt was made to obtain normalized gain measurements and the results are summarized in Table 4.

The mirror scan antenna was moved and reinstalled in close proximity to the *C*-band AN/SPS-10 radar. This system had been modified to permit the radar transmitter/receiver to be switched manually between its antenna and the mirror scan antenna. A second radar with similar power and pulse characteristics was installed to provide an operational capability at *X*-band. Both systems were modified to permit operation from a common pulse repetition frequency (prf) generator. For reference and orientation, the plan position indicator (PPI) display of the normal AN/SPS-10 is shown in Fig. 24. The displayed range is 25 nmi. The site overlooks the Chesapeake Bay area and the contours of the eastern shore are readily discernable. The display also shows the low elevation blockage to the west which is normally experienced at the site. The mirror scan parabolas were installed and oriented approximately NE and SE, that is at 045° and 135°.

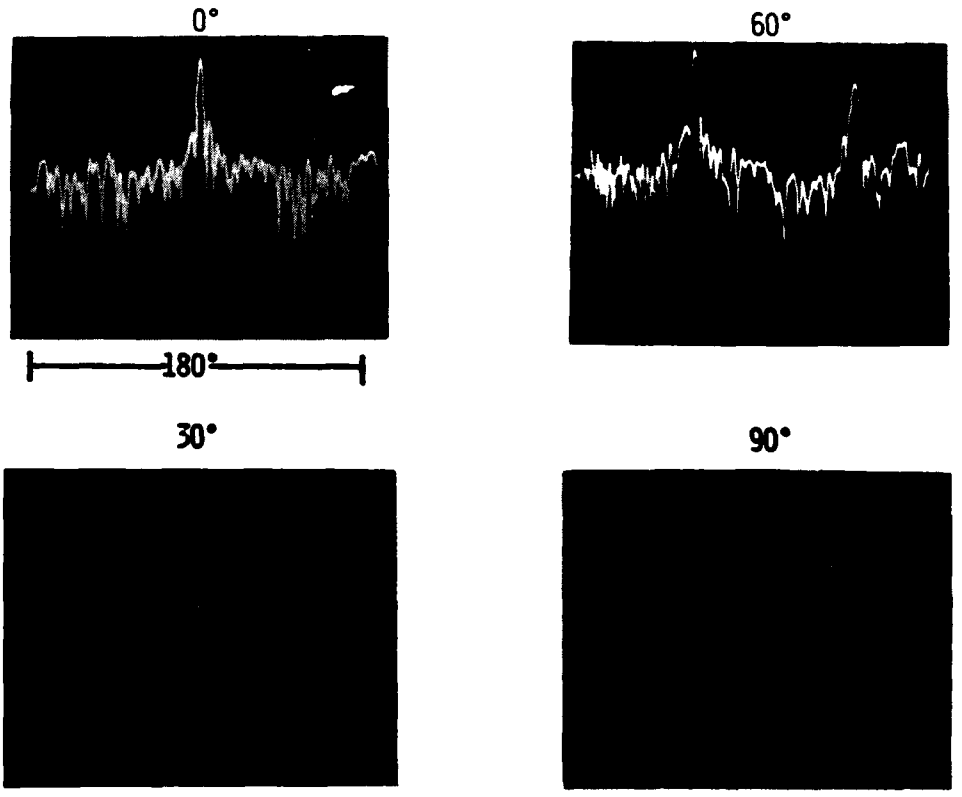

Fig. 18 — Azimuth antenna patterns for four fixed mirror scanned angles taken at 5.0 GHz

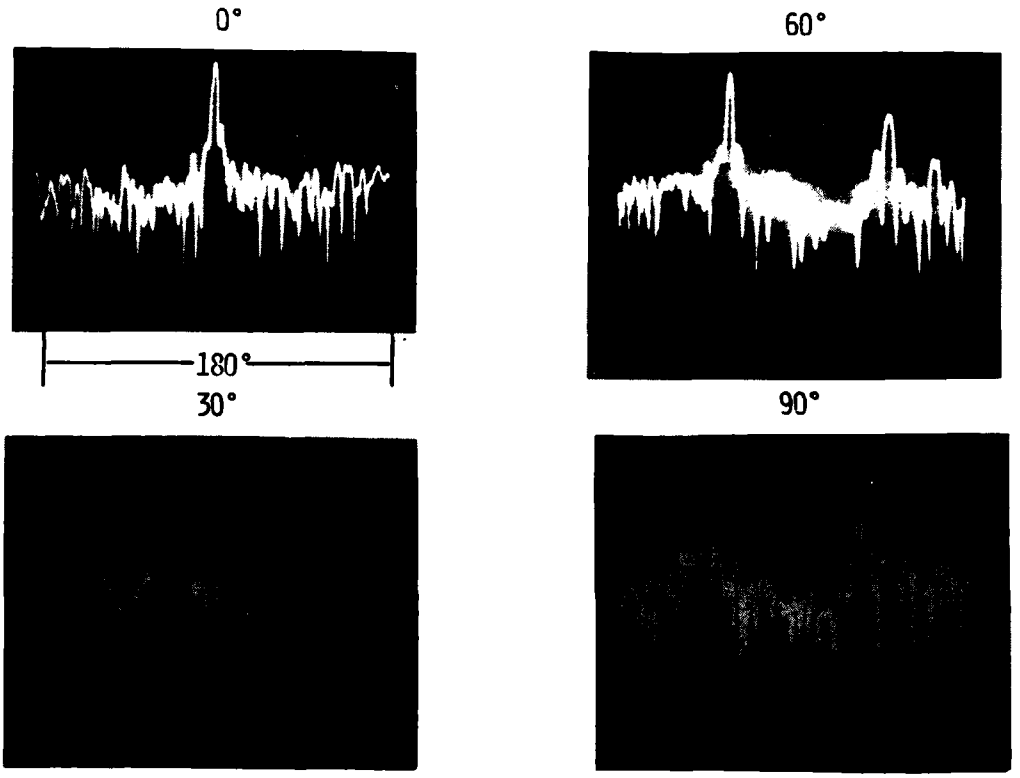

Fig. 19 — Azimuth antenna patterns for four fixed mirror scanned angles taken at 5.5 GHz

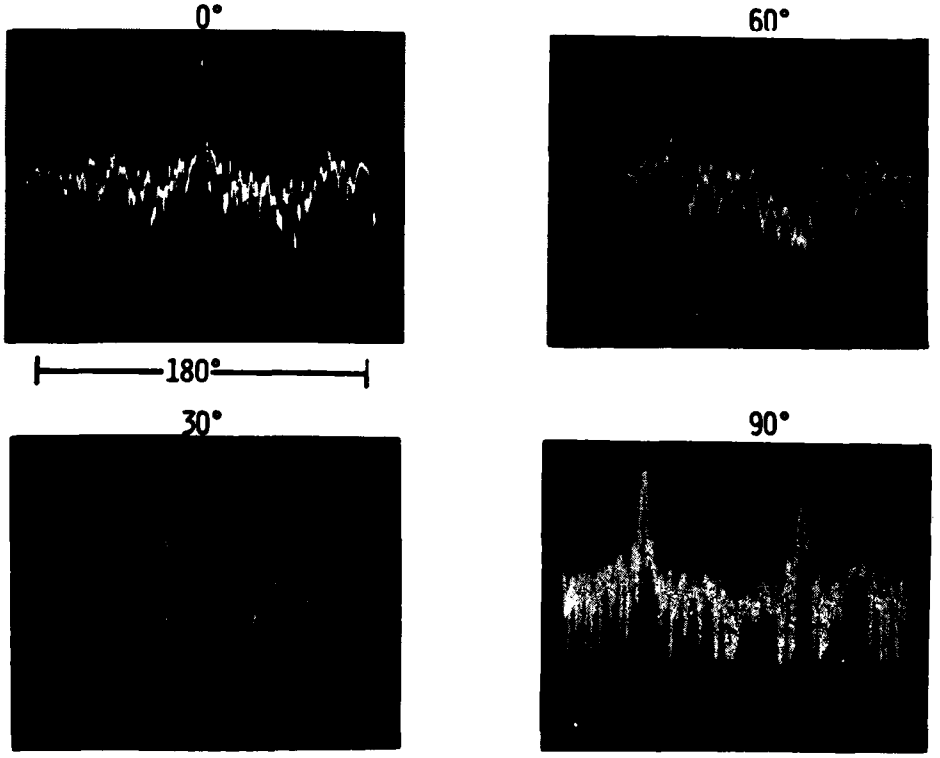

Fig. 20 — Azimuth antenna patterns for four fixed mirror scanned angles taken at 6.0 GHz

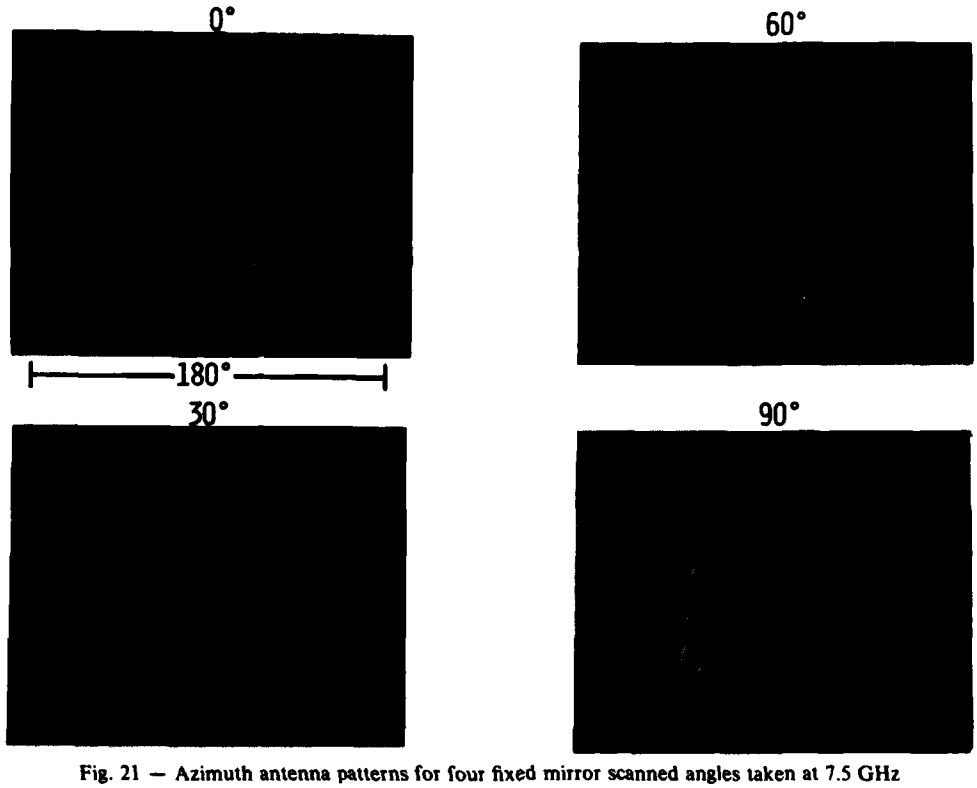

Fig. 21 — Azimuth antenna patterns for four fixed mirror scanned angles taken at 7.5 GHz

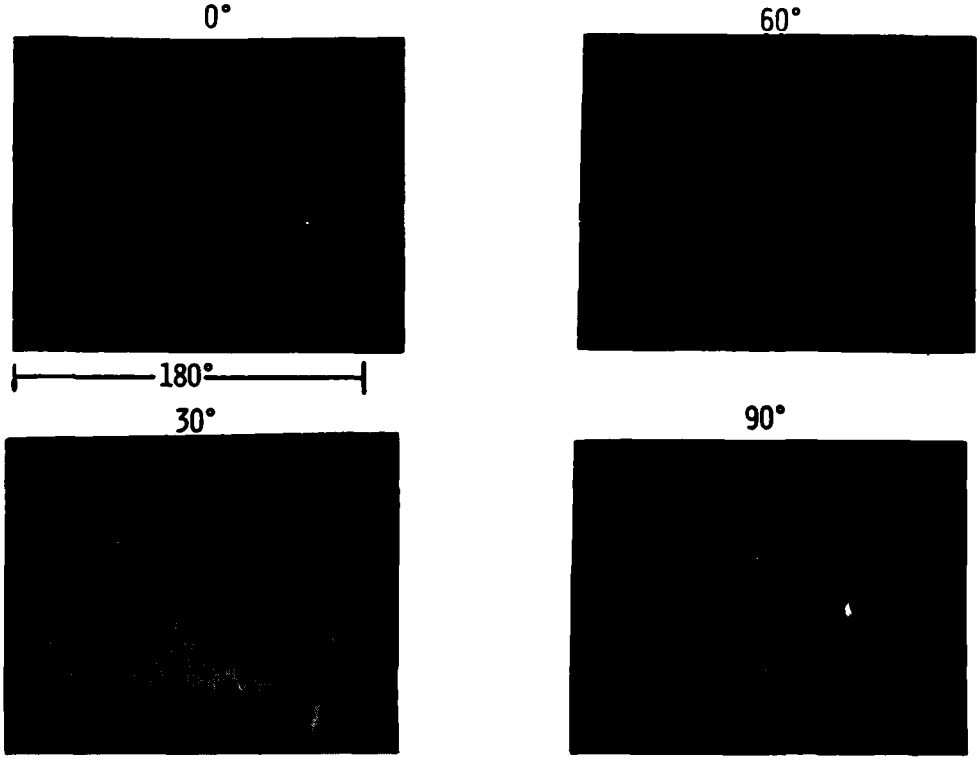

Fig. 22 — Azimuth antenna patterns for four fixed mirror scanned angles taken at 8.5 GHz

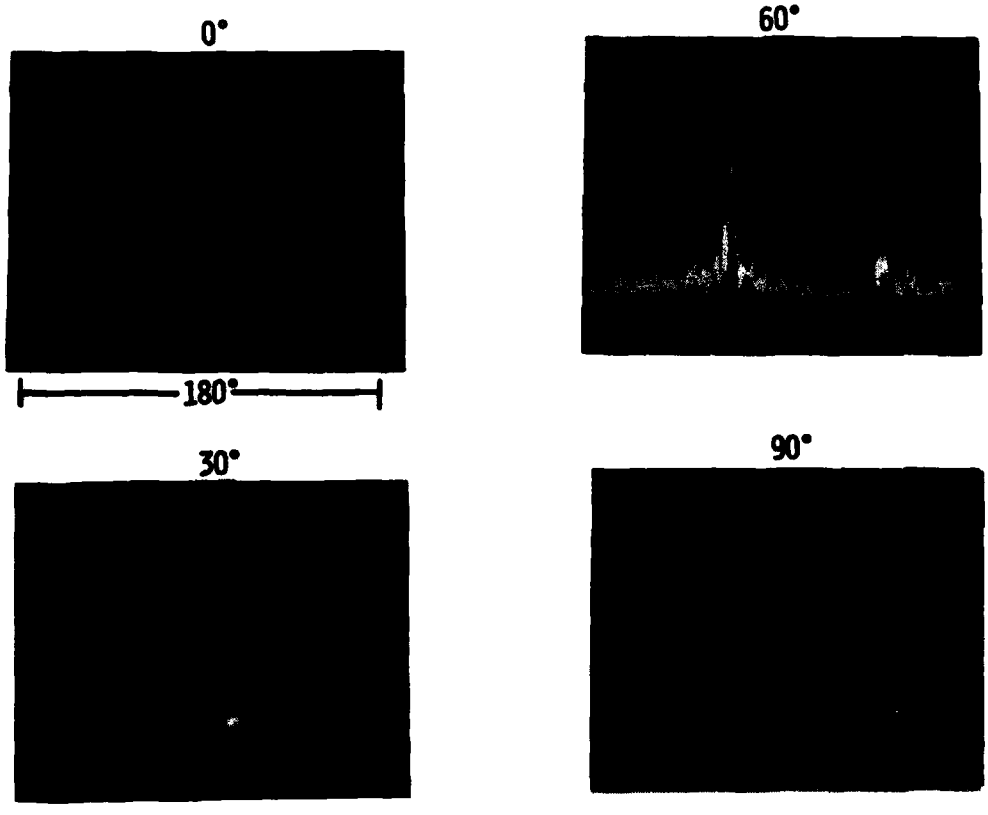

Fig. 23 — Azimuth antenna patterns for four fixed mirror scanned angles taken at 9.5 GHz

Table 4 — Normalized Antenna Gains as a Function of Frequency and Mirror Scan Angle

	Frequency (MHz)										
Angle (Degrees)	4500	5000	5500	6000	6500	7000	7500	8000	8500	9000	9500
0	27.8	28.2	28.6	29.2	30.1	29.6	31.7	34.0	32.7	35.7	33.0
30	26.8	—	28.8	—	29.9	—	31.4	—	31.8	—	32.5
60	25.9	—	28.3	—	29.3	—	29.6	—	31.3	—	31.5
90	25.0	—	27.2	—	29.5	—	29.4	—	30.0	—	26.2

Fig. 24 — Single scan PPI display of AN/SPS-10 video

The antenna interface to the two radars consisted of a pair of electromechanical waveguide switches and control circuitry to switch each radar between the two parabola-feed combinations. For multiplex operation, triggers for the switch control voltages were derived from the continuously rotating mirror. On each revolution, one trigger occurs when the mirror face is oriented halfway between the two parabolas (90°) and switches radar operation from the NE to the SE parabola. The second, and less critical, trigger occurs when the mirror rotation reaches 270° and resets operation back to the NE parabola. The two triggers are also used to blank radar transmissions during the time the switches are in operation. Provisions were also made to permit manual selection of either parabola for continuous operation.

One of the disadvantages of the mirror scan concept was noted earlier. Additional data processing would be required to adapt the data from the two stacked (azimuthally squinted) beams for display on a conventional PPI. It was felt that this increased complexity and cost was not required for demonstrating the antenna concept, and two synchros were installed in the pedestal to provide sweep inputs for a PPI display. Both require two-to-one gearing since the beam scanning rate is twice that of the mirror. Two electrical outputs, offset by 90°, are necessary to define the projected mean of the two beam positions with respect to each of the quadrature parabola-feed combinations.

The PPI display of the *C*-band mirror scan operation is shown in Fig. 25. Displayed are representative scans showing continuous operation with each single parabola and multiplexed operation with both. Clutter details compare favorably with those of the normal AN/SPS-10. Since no effort was made to blank the radar transmissions, large clutter returns are seen well past the 180° coverage normally provided by a single parabola. Since a short persistence tube was used in the display, the occurrence of the back-to-back scan during multiplex operation is not readily discernable. The same comments are applicable to the display of *X*-band operation shown in Fig. 26. The expected rotational displacement between the returns from the squinted *C*- and *X*-band beams is readily apparent. Although data are not shown, simultaneous operation with both radars operating at full power was satisfactorily demonstrated.

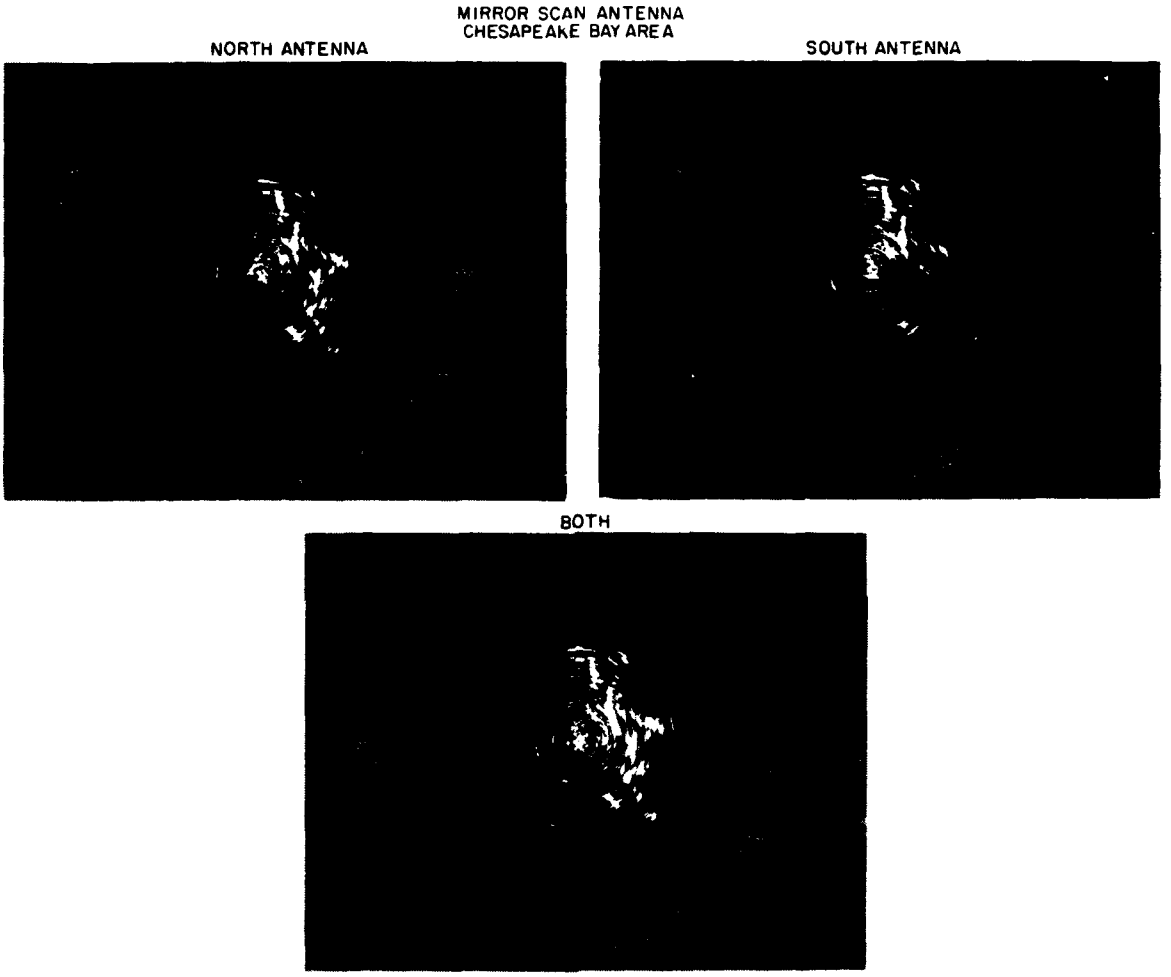

Fig. 25 — PPI video display of mirror scan antenna operation at C-band

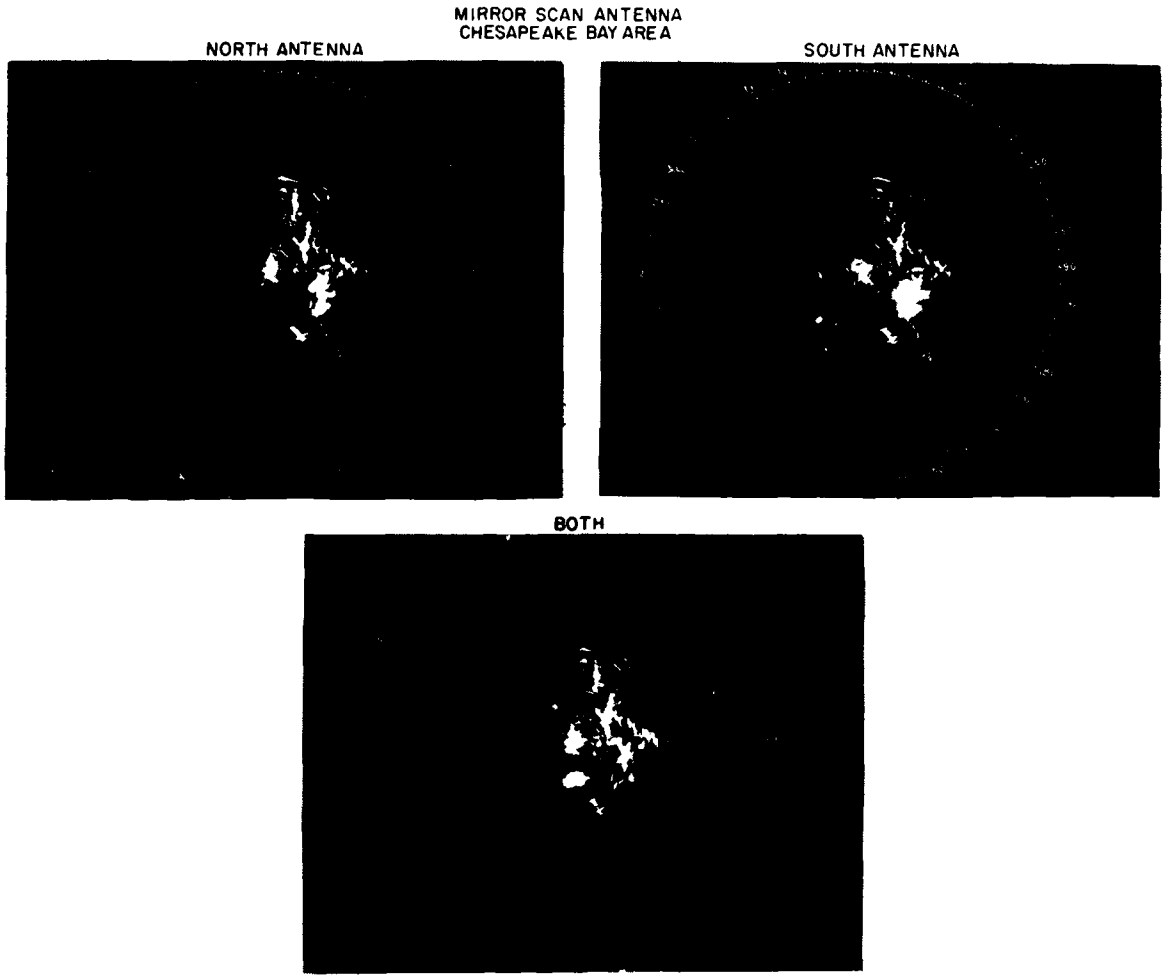

Fig. 26 — PPI video display of mirror scan operation at X-band

SUMMARY AND CONCLUSIONS

A new type of surveillance radar antenna was developed by NRL that eliminates all electrical rotary joints or slip rings. The only moving part in this antenna is a flat mirror that rotates about a vertical axis and transforms vertically to horizontally polarized radiation. This antenna permits multiple simultaneous beams to be formed via fixed feeds in the focal planes of four unipolar parabolas that illuminate the flat mirror from orthogonal directions. The multiple beams can also be used for sharing the antenna between multiple radars operating at different frequencies.

A model of this antenna was developed and tested. The antenna was designed to cover the frequency range from 2-10 GHz and met these specifications under test.

A prototype antenna was fabricated and used to demonstrate simultaneous operation with two radars. One radar was the SPS-10 operating at *C*-band and the other was an *X*-band surveillance radar. Switching circuits permitted the SPS-10 to be switched back and forth between its own antenna and the mirror scanned antenna for comparison purposes. In addition, the two radar outputs were multiplexed onto a single PPI display where they could be observed sequentially or simultaneously. In these tests the antenna met all expectations.

The prototype NRL two-reflector mirror-scan antenna was sent to NOSC in 1977, where it was carefully tested. The results of that test program are described in NOSC Technical Note 641, by A. D. Munger [9].

ACKNOWLEDGMENTS

The authors express appreciation to S. J. Weller for his assistance in obtaining the antenna patterns and to M. J. Siegert for his assistance in the antenna measurements, the servo implementation, and the radar modifications.

REFERENCES

[1] B.L. Lewis, "360° Azimuth Scanning Antenna Without Rotating R. F. Joints," U.S. Patent No. 3,916,416, 28 Oct. 1975.

[2] M.I. Skolnik, "Radar Handbook," New York: McGraw-Hill Book Co., 1970.

[3] G.V. Trunk, "Tracking Accuracy of the Mirror Scan Antenna in a 2D Configuration," NRL Report 7982, Apr. 5, 1976, pp. 10-11.

[4] P.W. Hannan, "Microwave Antennas Derived From the Cassegrain Telescope," IRE Trans. Ant. and Prop. AP-21, 140-153, Mar. 1961.

[5] L. Young, L.A. Robinson, and C.A. Hacking, "Meander-Line Polarizer," IEEE Trans. Ant. and Prop. AP-21, 376-378, May 1973.

[6] J.P. Shelton, "Wideband Polarization-Transforming-Electromagnetic Mirror," U.S. Patent No. 4,228,437, 14 Oct. 1980.

[7] R.H. DuHamel and M.E. Armstrong, "Log-Periodic Transmission Line Circuits—Part I: One Port Circuits," IEEE Trans., MTT, MTT-14, 264-274, June 1966.

[8] B.L. Lewis, "Efficient Wide-Angle Coverage Dipole Van Atta Array Design," IEEE Trans. Ant. and Prop., Vol. Ap-16, Mar. 1968, pp. 256.

[9] A.D. Munger, "Mirror Scan Antenna Analysis and Design," NOSC TN 641, Apr. 1979.

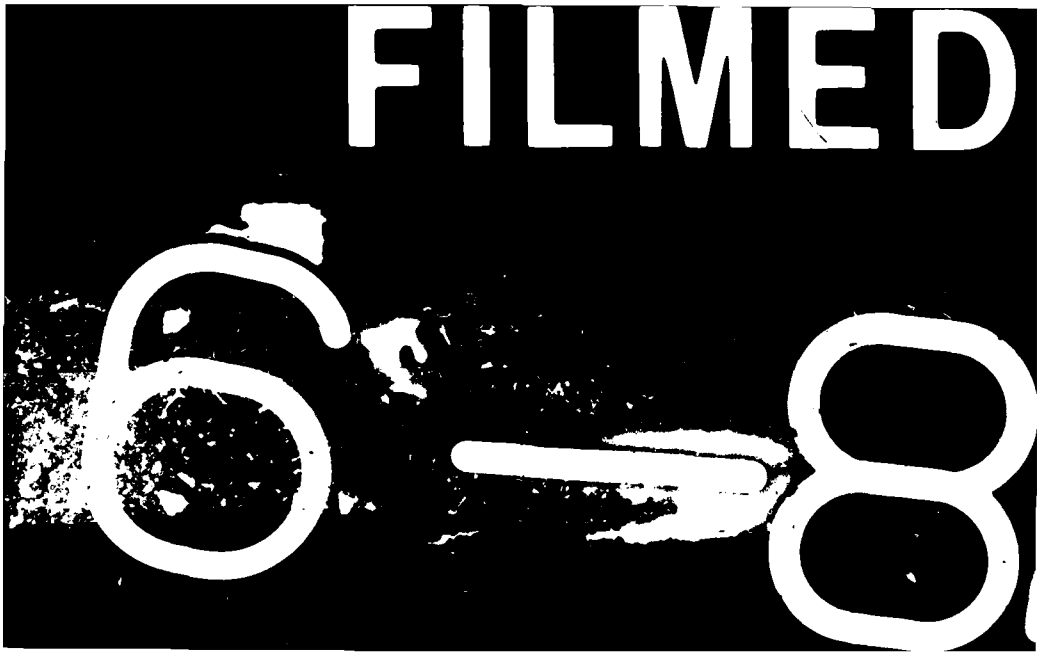
FILMED
6-8